DOI https: //doi. org/10.1007/s11595-019-2181-0

5*H*-Fluoreno [3,2- b:6,7- b'] Dithiophene Based Non-fullerene Small Molecular Acceptors for Polymer Solar Cell Application

WU Jiansheng, WANG Wei, ZHAN Chun, XIAO Shengqiang*

(State Key Laboratory of Advanced Technology for Materials Synthesis and Processing, Wuhan University of Technology, Wuhan 430070, China)

Abstract: Two novel non-fullerene small molecule acceptors were prepared with the conjugated backbone of 5*H*-fluoreno[3,2-b:6,7-b']dithiophene carrying the electron deficient unit of dicyanomethylene indanone (DICTFDT) and rhodanine (TFDTBR), respectively. The two acceptors exhibited excellent thermal stability and strong absorption in the visible region. The LUMO level is estimated to be at −3.89 eV for DICTFDT and −3.77 eV for TFDTBR. When utilized as the acceptor in bulk heterojunction polymer solar cells with the polymer donor of PBT7-Th, the optimized maximum power conversion efficiency of 5.12% and 3.95% was obtained for the device with DICTFDT and TFDTBR, respectively. The research demonstrates that 5*H*-fluoreno[3,2-b:6,7-b']dithiophene can be an appealing candidate for constructing small molecular electron acceptor towards efficient polymer:non-fullerene bulk heterojunction solar cells.

Key words: polymer solar cells; bulk heterojunction; non-fullerene acceptor

1 Introduction

Tremendous attention have been attracted world-widely by polymer solar cells (PSCs) because of their potential advantages of low cost, light weight, flexibility and large-scale production[1-5]. Power conversion efficiency (PCE) has been continuously paved forward along with renewing active components, optimizing corresponding morphologies and tuning the device interfaces within the bulk heterojunction (BHJ) blends of PSCs[6]. The active layer of a BHJ PSC device typically consists of a blend of a polymer donor and an electron acceptor. Fullerene derivatives, such as $PC_{71}BM$ and $PC_{61}BM$, have been working as the most common acceptors for organic solar cells owing to their high electron affinity, isotropic charge transport and formation of appropriate phase separation[7, 8]. The maximum PCE up to 12% has been achieved for single junction polymer:fullerene BHJ PSCs[9]. However, fullerene acceptors have intrinsic limitations of high synthetic cost, poor morphological stability, weak absorption in the visible region, and low tunability on energy levels. Alternatively, non-fullerene small molecular acceptors have therefore been attracting increasing attention in recent years because of their easily tunable optoelectronic properties by molecular engineering[10,11]. Since the report of the non-fullerene acceptor of ITIC with dicyanomethylene indanone subunit by Zhan in 2015[12], many dicyanomethylene indanone based acceptors have emerged and afforded excellent photovoltaic performance for the devices based on these materials[13-22]. The maximum PCE even approaches up to 13% for a single bulk heterojunction PSC device based on this type of acceptors[23].

Dicyanomethylene indanone based non-fullerene acceptors are the most studied candidates so far because of their strong electron withdrawing capability and relatively high electron mobility. For these successful non-fullerene acceptors, dicyanomethylene indanone and rhodanine units have been introduced as end groups attaching to the ladder-type conjugated centers. On the other hand, fluorene has been dominantly employed to construct ladder-type conjugated backbones with superior optoelectronic properties. Some acceptors based on fluorene and dicyanomethylene indanone units have been reported with comparable photovoltaic performance to fullerene acceptors [24]. The out-of-plane alkyl side chains on the tetrahedral carbon atom of fluorene offer sufficient solubility of materials for solution processability. Furthermore, by fusing heterocyclic aro-

(Received: Aug. 18, 2018; Accepted: July 25, 2019)

WU Jiansheng(吴建生): E-mail: m15377036978@163.com

*Corresponding author: XIAO Shengqiang (肖生强): Prof.; Ph D; E-mail: shengqiang@whut.edu.cn

Funded by the National Natural Science Foundation of China (No. 21673170)

matics to fluorene can enlarge the π-conjugation of the backbone, which has been proven helpful to improve device performance.

Herein, we report two small molecule acceptors based on 5*H*-fluoreno[3,2-b:6,7-b']dithiophene unit fusing a fluorene unit with a thiophene unit at both of its ends. Flanking electron deficient dicyanomethylene indanone and rhodanine sub units to both ends of the 5*H*-fluoreno[3,2-b:6,7-b']dithiophene unit afforded two non-fullerene small molecular acceptors of DICTFDT and TFDTBR, respectively. The 5*H*-fluoreno[3,2-b:6,7-b']dithiophene unit is employed as a rigid aromatic core with enlarged conjugation, which is beneficial to facilitating device charge transport. What's more, it also offers a way to tune the solubility and crystallinity of the materials in solid state through varying the alkyl chains at the tetrahedral center[24]. The optical and electrochemical properties of DICTFDT and TFDTBR were investigated as well as the photovoltaic performance in conjugation with their solid-state structures. The PCEs of 5.12% and 3.95% were obtained for the devices with DICTFDT and TFDTBR, respectively, when PTB7-Th was used as the polymer donor[25].

2 Experimental

3,6-bromofluorene was synthesized according to the reported procedure[26]. Other chemicals used were purchased from J&K, Energy Chemical, Sinopharm Chemical Reagent Co. Ltd., *etc*.. THF and toluene were distilled before used. General experimental information on chemical structure characterization, measurements of thermal stability, light absorption and electrochemical properties, polymer:non-fullerene acceptor BHJ solar cell device fabrication and characterizations can be found from our previous publications[25].

2.1 7-(4-hexylthiophen-2-yl)benzo[c][1,2,5]thiadiazole-4-carbaldehyde

7-bromobenzo[c][1,2,5]thiadiazole-4-carbaldehyde (486 mg, 2.0 mmol), tributyl(4-hexylthiophen-2-yl)stannane (1.14 g, 2.50 mmol), $Pd(PPh_3)_4$ (69 mg, 0.06 mmol) were sequentially added into a two-necked flask under N_2 before 15 mL of anhydrous toluene was injected in. The mixture was heated to reflux for 12 hours. After cooling down to room temperature, the solvent was removed by rotary evaporation under reduced pressure. The crude product was purified by silica gel column chromatography using petroleum ether/ ethyl acetate (10:1, *v/v*) as the eluent to get 585.0 mg of yellow solid product (89% yield). ^{1}H NMR (500 Hz, $CDCl_3$) δ (ppm): 10.72 (s, 1H), 8.22 (d, J = 7.6 Hz, 1H), 8.16 (s, 1H), 7.98 (d, J = 7.5 Hz, 1H), 7.19 (s, 1H), 2.71 (t, J = 7.5 Hz, 2H), 1.70 (t, J = 7.5 Hz, 2H), 1.34 (m, 6H), 0.92-0.89(m, 3H); ^{13}C NMR (125 Hz, $CDCl_3$) δ (ppm):188.53, 153.74, 152.34, 144.95, 138.07, 133.34, 132.66, 131.61, 125.43, 124.60, 123.85, 31.64, 30.52, 30.43, 28.96, 22.59, 14.07.

2.2 7-(5-bromo-4-hexylthiophen-2-yl) benzo[c][1,2,5]thiadiazole-4-carbaldehyde

7-(4-hexylthiophen-2-yl)benzo[c][1,2,5]thiadiazole-4-carbaldehyde (585.0 mg, 1.78 mmol), 15 mL of chloroform and 15 mL of glacial acetic acid were added into a flask. NBS (317.0 mg, 1.78 mmol) was added under ice bath in batches. After the reaction was over, 50 mL of diluted NaOH solution was added and the mixture was extracted by dichloromethane (3 × 50 mL). The organic phase was dried over anhydrous $MgSO_4$. After concentrated under reduced pressure, the crude product was further purified by silica gel column chromatography using petroleum ether/ethyl acetate (10:1, *v/v*) as the eluent to give 674.0 mg of product as yellow solid (92.6% yield). ^{1}H NMR (500 Hz, $CDCl_3$) δ (ppm): 10.71 (s, 1H), 8.20 (d, J = 7.6 Hz, 1H), 7.93 (s, 1H), 7.90 (d, J = 7.5 Hz, 1H), 2.65 (t, J = 7.65 Hz, 2H), 1.67 (m, 2H), 1.43-1.35 (m, 6H), 0.90 (t, J = 6.8 Hz, 3H); ^{13}C NMR (125 Hz,$CDCl_3$) δ (ppm):188.33, 153.61, 152.00, 143.63, 137.61, 132.38, 132.10, 130.41, 125.54, 123.22, 115.02, 31.57, 29.65, 29.59, 28.88, 22.56, 14.05.

2.3 3,6-dibromo-9,9-di(2-ethylhexyl)-9*H*-fluorene

Under the protection of N_2, 3,6-dibromofluorene (12.96 g, 40 mmol), *n*-tetrabutylammonium iodide (4.54 g, 12.3 mmol) , DMSO (60 mL), and 50% NaOH (50 mL) were added to a two-necked flask. After the mixture was stirred sufficiently, 2-ethylhexyal bromide (100.0 mmol, 18.5 mL) was added into the flask. The reaction was stopped after heated at 100 ℃ for 3 hours. After cooling down to room temperature, 100 mL of water was added in and the mixture was extracted with petroleum ether (3×40 mL). The combined organic phase was dried over anhydrous $MgSO_4$ and filtered. After the removal of the solvent, the crude product was purified by column chromatography using petroleum ether as the eluent to obtain 21.45 g of the pure product as a clear colorless oil (97.8% yield). ^{1}H NMR (500 Hz, $CDCl_3$) δ (ppm): 7.78 (s, 2H), 7.42 (d, J = 9.1 Hz, 2H), 7.23 (d, J = 9.7 Hz, 2H), 1.93 (m, 4H), 0.95-0.87 (m, 8H), 0.82-0.70 (m, 12H), 0.50 (m, 8H), 0.42

(m, 2H);^{13}C NMR (125 Hz, $CDCl_3$) δ (ppm):149.40, 141.99, 129.89, 125.49, 123.09, 120.82, 54.73, 44.26, 34.49, 33.68, 28.06, 26.84, 22.65, 13.93, 10.16.

2.4 3,6-dibromo-2,7-diiodo-9,9-di(2-ethylhexyl)-9*H*-fluorene

3,6-dibromo-9,9-di(2-ethylhexyl)-9H-fluorene (5.48 g, 10.0 mmol), periodic acid (3.42 g, 15.0 mmol), iodine (1.40 g, 5.5 mmol) were added to a 500 mL flask containing 150.0 mL of acetic acid, 6.0 mL of water, 2.7 mL of sulfuric acid. The mixture was heated at 80 ℃ under stirring for 1 hour and another part of iodine (1.40 g, 5.5 mmol) was added. After reacting for another 2 hours, the mixture was cooled down to room temperature and quenched with 100 mL of diluted NaOH solution. After extracting with petroleum ether (3 × 30 mL), the organic phase was dried over anhydrous $MgSO_4$ and filtered. After concentrated in reduced pressure, the crude product was purified by silica gel column chromatography using petroleum ether as the eluent to give 7.61 g of liquid product (95% yield). ^{1}H NMR (500 Hz, $CDCl_3$) δ (ppm): 7.90 (s, 2H), 7.85 (s, 2H), 1.89 (m, 4H), 0.94 (m, 8H), 0.84-0.78 (m, 12H), 0.56 (m, 8H), 0.45 (m, 2H); ^{13}C NMR (125 Hz, $CDCl_3$) δ (ppm):150.90, 141.05, 135.89, 128.08, 123.97, 99.57, 54.79, 43.92, 34.79, 33.78, 28.08, 27.16, 22.78, 14.08, 10.28.

2.5 ((3,6-dibromo-9,9-di(2-ethylhexyl)-9*H*-fluorene-2,7-diyl)bis(ethyne-2,1-diyl))bis(trimethylsilane)

3,6-dibromo-2,7-diiodo-9,9-di(2-ethylhexyl)-9H-fluorene (8.0 g, 10.0 mmol), cuprous iodide (190.0 mg, 1.0 mmol), $Pd_2(PPh_3)_2Cl_2$ (350.0 mg, 0.5 mmol), 80 mL of trimethylamine were added to a 250 mL two-necked flask under N_2 before trimethylsilylacetylene (25.0 mmol, 2.55 mL) was added in. The reaction mixture was stirred at room temperature for 12 hours and then quenched with 10 mL of water. The mixture was extracted with petroleum ether (3 × 30 mL) and washed with diluted hydrochloric acid. The organic phase was dried over anhydrous $MgSO_4$ and filtered. After the removal of the solvent, the crude product was purified by silica gel column chromatography using petroleum ether as the eluent to obtain 6.22 g of brown-colored viscous liquid product (84% yield).^{1}H NMR (500 Hz, $CDCl_3$) δ (ppm): 7.84 (s, 2H), 7.46 (s, 2H), 1.92 (m, 4H), 0.98-0.89 (m, 8H), 0.81-0.71 (m, 12H), 0.57-0.52 (m, 10H), 0.29 (m, 18H); ^{13}C NMR (125 Hz,$CDCl_3$) δ (ppm):149.88, 140.94, 128.76, 124.62, 124.12, 123.78, 103.74, 100.12, 54.76, 44.28, 34.74, 33.42, 27.96, 27.10, 22.75, 14.02, 10.30, 10.28. MALDI-TOF MS for $C_{39}H_{56}Br_2Si_2$: calcd 740.84; found, 741.20 (M^+).

2.6 5,5-di(2-ethylhexyl)-5*H*-fluoreno[3,2-b:6,7-b']dithiophene

Under the protection of nitrogen, ((3,6-dibromo-9,9-di(2-ethylhexyl)-9H-fluorene-2,7-diyl) bis(ethyne-2,1-diyl))bis(trimethylsilane) (233.0 mg, 0.30 mmol) and sodium sulfide nonahydrate (432.0 mg, 1.8 mmol) were added to a 100 mL two-necked flask before 20 mL of NMP was injected in. After heated at 180 ℃ for 12 hours, the mixture was cooled to room temperature, added in 50 mL of water and extracted with dichloromethane (3×50 mL). The combined organic phase was dried, filtered and concentrated under reduced pressure. The crude product was purified by silica gel column chromatography using petroleum ether as the eluent to give 124.0 mg of colorless oil product (82% yield).^{1}H NMR (500 Hz,$CDCl_3$) δ (ppm): 8.22 (s, 2H), 7.77 (d, J = 2.8 Hz, 2H), 7.42 (s, 2H), 7.34 (s, 2H), 2.10 (m, 4H), 0.89-0.66 (m, 18H), 0.59 (m, 6H), 0.48 (m, 6H); ^{13}C NMR (125 Hz, $CDCl_3$) δ (ppm): 147.72, 138.78, 138.45, 125.88, 123.89, 118.82, 113.13, 53.55, 45.68, 34.41, 32.85, 27.84, 26.92, 22.52, 13.77, 9.98. MALDI-TOF MS for $C_{33}H_{42}S_2$: calcd 502.8; found, 503.3 (M^+).

2.7 (5,5-dihexyl-5H-fluoreno[3,2-b:6,7-b']dithiophene-2,8-diyl)bis(tributylstannane)

5,5-di(2-ethylhexyl)-5H-fluoreno[3,2-b:6,7-b'] dithiophene (1.51 g, 3.0 mol) and 30 mL of anhydrous THF were added to a flame-dried two-necked flask under N_2. Then 2.4 M *n*-BuLi in hexane (3.0 mL, 7.2 mmol) was added dropwisely at −78 ℃. After 40 minutes, 2.10 mL of tri-*n*-butyltinchloride was added in. The reaction was then gradually warmed to room temperature and stirred for another 4 hours before quenched with water. After the mixture was extracted with ether (3×30 mL), the combined organic phase was dried over anhydrous $MgSO_4$, filtered and concentrated. The crude product was used directly in the next step without further purification.

2.8 TFDTB-CHO

To a 50 mL two-necked flask was added 7-(5-bromo-4-hexylthiophen-2-yl)benzo[c][1,2,5]thiadiazole-4-carbaldehyde (634.0 mg, 1.55 mmol), (5,5-dihexyl-5H-fluoreno[3,2-b:6,7-b']dithiophene-2,8-diyl) bis(tributylstannane) (695.0 mg, 0.65mmol) and $Pd(PPh_3)_4$ (37.0 mg, 0.032 mmol) under the protection of nitrogen before 10 mL of anhydrous toluene was injected in. After refluxed overnight, the mixture

was cooled to room temperature and the solvent was removed under reduced pressure. The crude product was purified by silica gel column chromatography using dichloromethane as the eluent to obtain 523.0 mg of yellow solid (70% yield). ^{1}H NMR (500 Hz, $CDCl_3$) δ (ppm): 10.72 (s, 2H), 8.21 (d, J = 7.5 Hz, 2H), 8.18 (t, J = 2.9 Hz, 2H), 8.15 (s, 2H), 7.97 (d, J = 7.5 Hz, 2H), 7.78 (t, J = 5.3 Hz, 2H), 7.53 (t, J = 3.45 Hz, 2H), 2.98 (m, 4H), 2.13 (m, 4H), 1.81 (m, 4H), 1.50 (m, 4H), 1.38 (m, 8H), 0.93-0.71 (m, 24H), 0.63 (m, 6H), 0.55 (m, 6H); ^{13}C NMR (125 Hz,$CDCl_3$) δ (ppm):188.32, 153.74, 152.18, 148.61, 139.46, 138.78, 135.49, 133.42, 132.36, 125.32, 123.48, 122.79, 122.76, 118.95, 118.85, 118.73, 112.83, 53.91, 45.71, 34.70, 33.55, 31.67, 30.55, 29.72, 29.31, 27.85, 26.90, 22.64, 14.09, 13.89, 10.25. MALDI-TOF MS for $C_{67}H_{74}N_4O_2S_6$: calcd 1 159.7; found, 1 159.5 (M^+).

2.9 TFDTBR

To a 250 mL two-necked flask was added TFDTB-CHO (348.0 mg, 0.3 mmol) and 3-ethylrhodanine (193.0 mg, 1.2 mmol) under N_2 before 100 mL of chloroform and 0.3 mL of piperidine were injected in. After the reactant was refluxed for 12 hours, the reaction was stopped and the solvent was removed under reduced pressure. The crude product was purified by silica gel column chromatography using chloroform as the eluent to afford 220.0 mg of pure solid product (50% yield). ^{1}H NMR(500 Hz, $CDCl_3$) δ (ppm): 8.30 (t, J = 5.9 Hz, 2H), 7.97 (m, 2H), 7.90 (d, J = 5.1 Hz, 2H), 7.78 (t, J = 6.4 Hz, 2H), 7.70 (m, 2H), 7.49 (s, 2H), 7.46 (d, J = 2.4 Hz, 2H), 4.20 (m, 4H), 2.87 (m, 4H), 2.15 (m, 4H), 1.77 (m, 4H), 1.50 (m, 4H), 1.39 (m, 8H), 1.32(m, 6H), 0.96-0.79 (m, 24H), 0.67 (m, 6H), 0.58 (m, 6H); ^{13}C NMR (125 Hz, $CDCl_3$) δ (ppm): 192.69, 167.24, 154.07, 151.23, 148.48, 141.37, 139.50, 139.21, 138.60, 136.39, 135.92,135.33, 132.45, 130.65, 128.39, 126.26, 124.54, 124.33, 123.80, 122.05, 118.62, 112.84, 53.89, 45.66, 39.88, 34.73, 33.60, 31.78, 30.36, 29.82, 29.67, 27.87, 22.86, 22.72, 14.16, 14.01, 12.27, 10.30. MALDI-TOF MS for $C_{77}H_{84}N_6O_2S_{10}$: calcd 1 446.2; found, 1 445.6 (M^+).

2.10 TFDT-CHO

(5,5-dihexyl-5H-fluoreno[3,2-b:6,7-b']dithiophene-2,8-diyl)bis(tributylstannane) (540.0 mg, 0.5 mol), 5-bromo-4-hexylthiophene-2-carbaldehyde (344.0 mg, 1.25 mmol), $Pd(PPh_3)_4$ (28.0 mg,0.025 mmol) were added to a flame-dried 25 mL two-necked flask under N_2.Then 10 mL of anhydrous toluene was injected into the flask. After refluxed overnight, the reaction mixture was cooled to room temperature. After the removal of the solvent, the crude product was purified by silica gel column chromatography using petroleum ether/ethyl acetate (10:1, *v/v*) as the eluent and then recrystallized in petroleum ether/dichloromethane to give 330.0 mg of yellow crystalline solid (74% yield). ^{1}H NMR (500 Hz, $CDCl_3$) δ (ppm) 9.87 (s, 2H), 8.18 (s, 2H), 7.78 (s, 2H), 7.64 (s, 2H),7.53 (d, J = 3.0 Hz, 2H), 2.92 (m, 4H), 2.10 (m, 4H), 1.74 (m, 4H), 1.44 (m, 4H), 1.34 (m, 8H), 0.90-0.65 (m, 24H), 0.59 (m, 6H), 0.51 (m, 6H); ^{13}C NMR (125 Hz, $CDCl_3$) δ (ppm): 182.53, 148.82, 141.37, 141.32, 141.15, 141.05, 139.74, 139.14, 139.04, 138.91, 134.88, 124.06, 119.20, 112.92, 53.93, 45.69, 34.69, 33.47, 31.57, 30.36, 29.46, 29.12, 27.91, 26.96, 22.62, 14.01, 13.81, 10.21. MALDI-TOF MS for$C_{55}H_{70}O_2S_4$: calcd 890.4; found, 891.5 (M^+).

2.11 DICTFDT TFDT-CHO

(178.0 mg, 0.2 mmol) and 2-(1,3-dioxo-1H-inden-2(3H)-ylidene)malononitrile (117.0 mg, 0.6 mmol) were added to a 250 mL two-necked flask under the protection of N_2. Then chloroform (100 mL) and pyridine (1 mL) were added via syringe. After refluxed for 12 hours, the solvent was removed via rotary evaporation. The crude product was purified by silica gel column chromatography with chloroform and then recrystallized in petroleum ether/dichloromethane to obtain 168.0 mg of pure product as a yellow crystalline solid (67% yield).^{1}H NMR (500 Hz, $CDCl_3$) δ (ppm): 8.66 (s, 2H), 8.58 (s, 2H), 7.92 (s, 2H), 7.85 (s, 4H),7.74 (s, 2H), 7.67 (s, 4H), 7.57 (d, J = 4.9 Hz, 2H), 2.83 (m, 4H), 2.19 (m, 4H), 1.72 (m, 4H), 1.46 (m, 4H), 1.37 (m, 8H), 0.93 (m, 24H), 0.67 (m, 6H), 0.60 (m, 6H); ^{13}C NMR (125 Hz, $CDCl_3$) δ (ppm): 187.94, 159.81, 149.02, 148.52, 147.58, 141.70, 140.51, 139.80, 139.38, 139.21, 136.90, 135.27, 135.09, 135.01, 134.38, 125.19, 124.81, 123.69, 122.56, 119.38, 114.36, 113.07, 69.69, 54.06, 45.64, 34.78, 33.67, 31.59, 30.01, 29.47, 29.36, 27.95, 22.96, 22.76, 22.59, 14.04, 13.92, 10.23. MALDI-TOF MS for $C_{79}H_{78}N_4O_2S_4$: calcd 1 243.7; found, 1 243.5 (M^+).

3 Results and discussion

3.1 Materials synthesis and optoelectronic properties

The synthetic routes of TFDTBR and DICTFDT are depicted in Scheme 1. Thermogravimetric analysis indicates that TFDTBR and DICTFDT have an excellent thermal stability with a 5% weight loss temperature (T_d) of 388 and 350 ℃ under N_2 atmosphere,

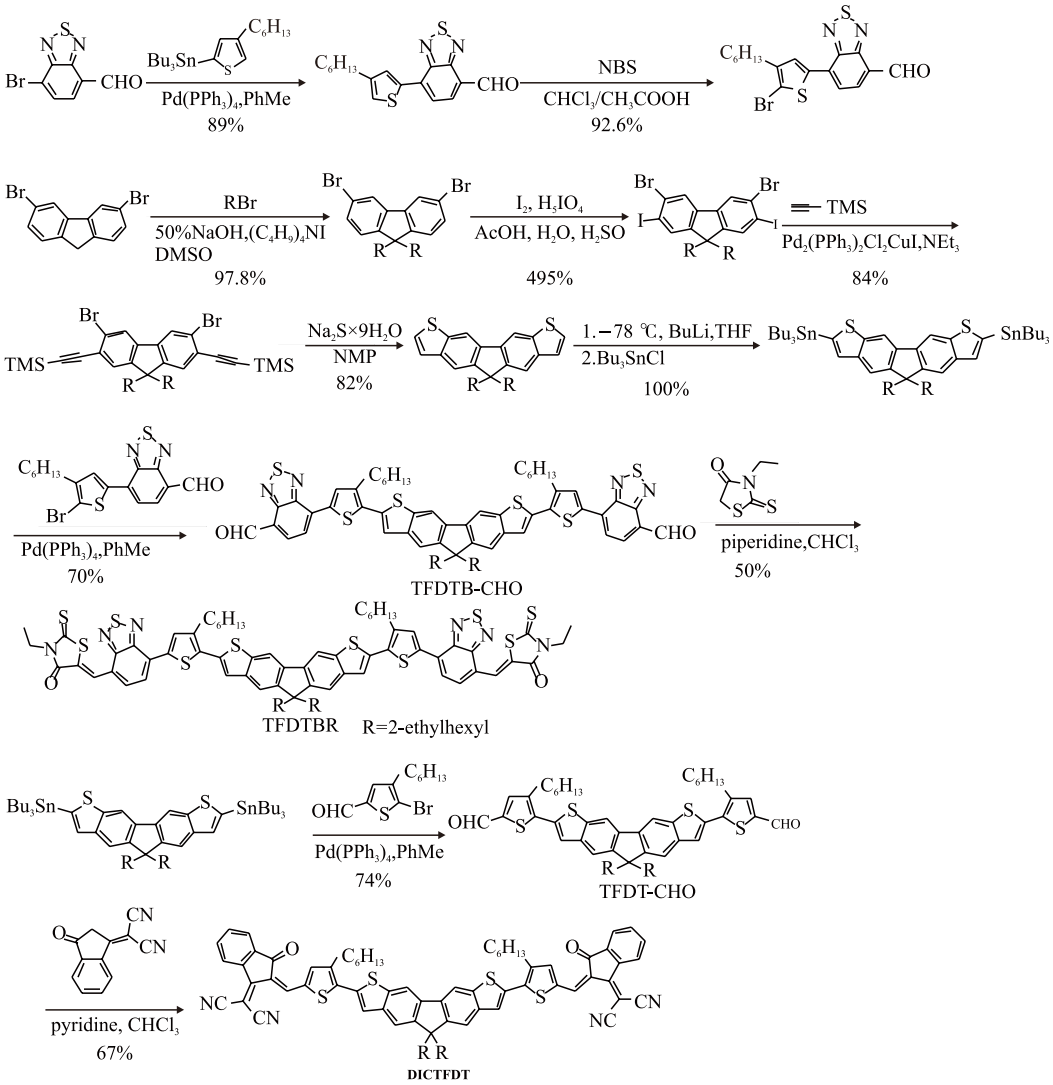

Scheme 1 Synthetic route of TFDTBR and DICTFDT

Table1 Optical and electrochemical properties of DICTFDT and TFDTBR

Acceptor	λ_{max}^{sol} /nm	λ_{max}^{film} /nm	E_g^{opt} /eV	E_{ox}^{onset} /V	HOMO/eV	LUMO/eV
DICTFDT	616	661	1.67	0.86	−5.56	−3.89
TFDTBR	563	602	1.69	0.78	−5.46	−3.77

respectively. They are both soluble in common organic solvents such as chloroform, toluene, chlorobenzene and o-dichlorobenzene at room temperature because of their solubilizing alkyl substituents. Good thermal stability and solubility ensure their processability for polymer solar cell device fabrication.

The UV-Vis absorption spectra of TFDTBR and DICTFDT are shown in Fig.1. In dilute o-dichlorobenzene (o-DCB) solution with a concentration of 1×10^{-5} M. DICTFDT exhibits an absorption peak at 618 nm with a maximum absorption coefficient of 0.91×10^5 M^{-1} cm^{-1}, while TFDTBR exhibits an absorption peak at 563 nm with a maximum absorption coefficient of 0.89×10^5 M^{-1} cm^{-1}. Compared to the absorption in solution, their film present red-shifted maximum absorption peak (λ_{max}) at 661 nm and 602 nm, respectively. Both films exhibit strong absorption in the range from 500 to 750 nm, which is beneficial to utilizing the solar light energy[27]. The electrochemical property of DICTFDT and TFDTBR was investigated by cyclic voltammetry (CV) method. The HOMO values were calculated from the onset voltages of oxidation ($E_{ox,onset}$), respectively, as presented in Table 1.The HOMO energy levels of DICTFDT and TFDTBR are found to be at −5.56 and −5.46 eV. The LUMO energy levels of DICTFDT and TFDTBR were estimated to be −3.89 eV and −3.77 eV according to $E_{LUMO} = (E_{HOMO} + E_g)$ eV, respectively.

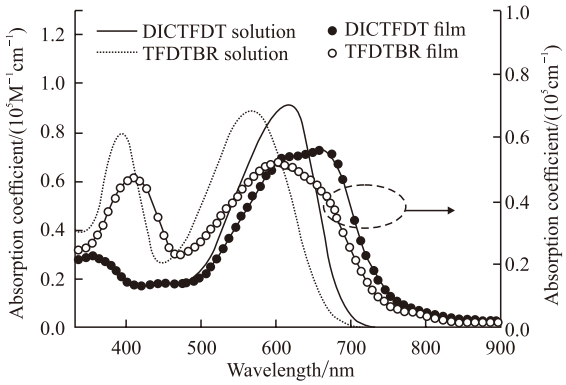

Fig.1 Absorption spectra of DICTFDT and TFDTBR in *o*-DCB solution and in film at room temperature

3.2 Solid state ordering

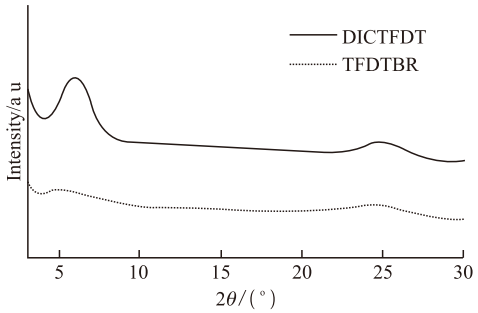

Fig.2 Powder XRD pattern of DICTFDT and TFDTBR

The crystallinity and stacking of the two small molecule acceptors in solids were investigated by powder X-ray diffraction (XRD). As shown in Fig.2, TFDTBR exhibits a weak crystal diffraction peak at 2θ=5.13° corresponding to a space value of 17.19Å dominated by the size of side chains. Nevertheless, DICTFDT has a much stronger diffraction peak at 2θ=6.07° with a space value of 14.54 Å, indicating closer stacking in alkyl chain direction for DICTFDT. At the same time, DICTFDT and TFDTBR present a diffraction peak at 2θ=25.68° and 24.84°, respectively, which is attributed to the π-π stacking between the conjugated backbones of the two acceptors. The corresponding calculated *d* spacing are 3.46 and 3.57 Å, respectively, which indicates that DICTFDT stacks more closely. The smaller π-π stacking distance of DICTFDT could be a result of enhanced intermolecular interactions, which would be favorable for charge transport in the PSCs. At the same time, it can also be observed that the π - π stacking diffraction intensity of DICTFDT is much stronger than that of TFDTBR, which reveals that the π-π stacking of DICTFDT is more ordered to give better crystallinity. Briefly, the crystallinity of DICTFDT and ordering are higher than those of TFDTBR, suggesting it could lead to better device performance.

3.3 Photovoltaic properties

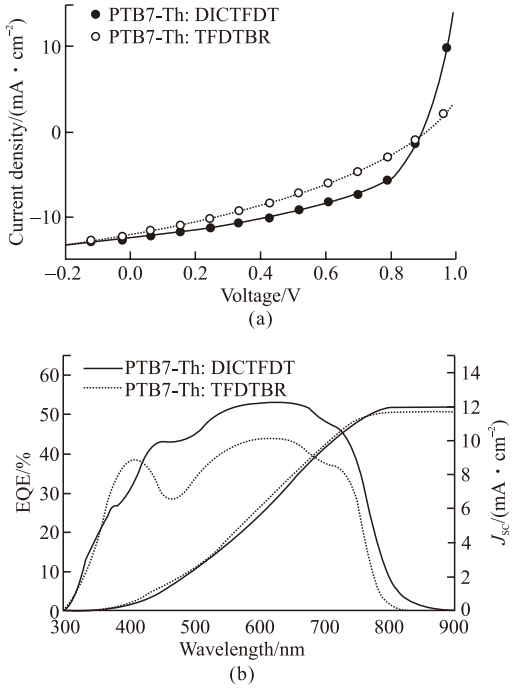

Fig.3 (a) The *J-V* curves of PSCs based on PTB7-Th:DICTFDT (2:3, *w/w*) and PTB7-Th:TFDTBR (2:3, *w/w*) under AM 1.5 G illumination(100 mW cm^{-2}); (b) The EQE curves of the optimized PTB7-Th:DICTFDT and PTB7-Th:TFDTBR devices

To evaluate the photovoltaic performance of the two acceptors, PTB7-Th was chosen as the polymer donor to fabricate polymer:non-fullerene acceptor BHJ PSCs. PSC devices were fabricated in the configuration of glass/ITO/ZnO/PTB7-Th: acceptor/MoO_3/Ag. The current density-voltage (*J-V*) curves of the optimized devices with D/A weight ratio of 2:3 and corresponding external quantum efficiency (EQE) spectra are provided in Fig.3. The device with the PTB7-Th:DICTFDT blend showed a maximum PCE of 5.12% (4.82% for average from 20 cells) with a V_{oc} of 0.89 V, a J_{sc} of 12.52 mA·cm^{-2} and an FF of 0.46 without any solvent additive processing or post-treatment. Meanwhile, the device based on the PTB7-Th:TFDTBR blend showed a maximum PCE of 3.95% (3.75% for average from 20 cells) with a V_{oc} of 0.92 V, a J_{sc} of 12.25 mA cm^{-2} and an FF of 0.35. Compared with the device of DICTFDT, from Fig.3(b), it can be seen that the PTB7-Th:DICTFDT device presents a stronger EQE over 43% in the wavelength range of 440-750 nm, with a maximum value of 53% at 623 nm. However, the PTB7-Th:TFDTBR device presents lower EQE values in the whole absorption range in comparison with the PTB7-Th:DICTFDT device. The integrated J_{sc}s from EQE spectra are 12.00 and 11.68 mA cm^{-2} for the device of PTB7-Th:DICTF-

DT and PTB7-Th:TFDTBR, respectively, consistent with the J_{sc} values measured under the irradiation of simulated AM 1.5 G sun light.

It is noted that the main contribution of the higher PCE value of the PTB7-Th:DICTFDT blend comes from its higher FF and slightly higher J_{sc} value. To better understand the performance distinction between the two devices, the photoluminescence (PL) of the two BHJ films were probed. The excitation wavelength of 688 nm was chosen for PTB7-Th while 670 nm for DICTFDT and 618 nm for TFDTBR according to their absorption spectra. As indicated in Fig.4(a), the PL of PTB7-Th is largely quenched by the acceptor (about 90%) in the PTB7-Th: DICTFDT film whereas only about 84% in the PTB7-Th: TFDTBR film. On the other hand, the PL of DICTFDT was quenched by PTB7-Th around 88% while only about 81% in the PTB7-Th: TFDTBR blend as shown in Fig.4(b). These results declare the light-harvesting contribution from both the donor and the acceptors and indicate that the exciton generation and dissociation are more efficient in the case of the PTB7-Th: DICTFDT blend.

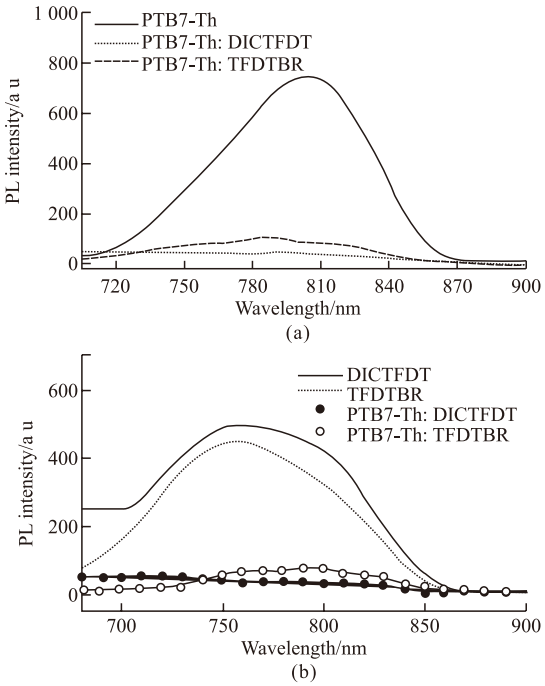

Fig.4 (a) Photoluminescence spectra of PTB7-Th, PTB7-Th:DICTFDT (2:3, *w/w*) and PTB7-Th:TFDTBR (2:3, *w/w*) excited at 688 nm and (b) DICTFDT, TFDTBR, PTB7-Th:DICTFDT (2:3, *w/w*) and PTB7-Th:TFDTBR (2:3, *w/w*) excited at 670 and 618 nm, respectively.

To investigate the influence of charge carrier transport on photovoltaic performances, the charge carrier mobilities of the PTB7-Th:DICTFDT and PTB7-Th: TFDTBR blends were determined by space charge limited current (SCLC) method with the device structure of ITO/ZnO/blend film/Ca/Al for electrons and ITO/ PEDOT:PSS/blend film/Al for holes. The PTB7-Th:DICTFDT blend yields a hole mobility (μ_h) of 0.73×10^{-4} cm^2 V^{-1}·s^{-1} and an electron mobility (μ_e) of 0.26×10^{-4} cm^2 V^{-1}·s^{-1}, whereas The PTB7-Th: TFDTBR blend offers a μ_h of 0.60×10^{-4} cm^2·V^{-1}·s^{-1} and a μ_e of 0.35×10^{-5} cm^2·V^{-1}·s^{-1}. The blend of DICTFDT:PTB7-Th exhibits higher charge carrier mobility and more balanced charge transport (μ_h/μ_e=2.81 *vs* 17.40), which is consistent with the higher FF of the device.

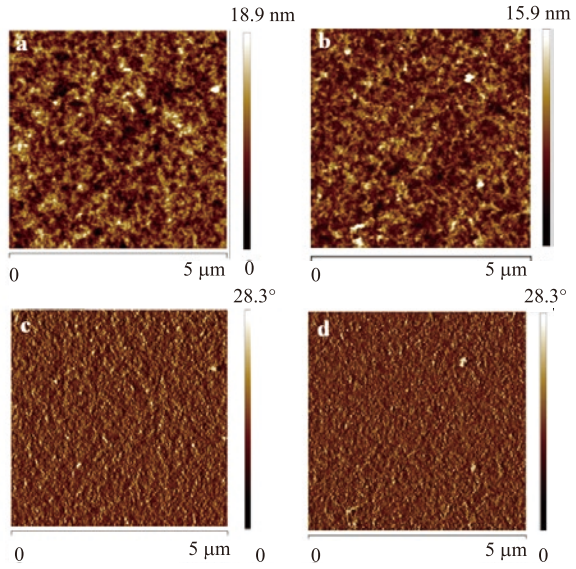

Fig.5 Tapping mode AFM height images of the optimized PTB7-Th: DICTFDT (a) and PTB7-Th: TFDTBR blend (b), and their corresponding phase images (c) and (d)

The morphology of the two blend films was probed by atomic force microscopy (AFM). As shown in Fig.5, the two BHJ blend films present little difference on the film microstructure. However, the root-mean-square (RMS) surface roughness is 3.08 nm for the active layer of PTB7-Th:DICTFDT while it is 2.23 nm for PTB7-Th:TFDTBR. Rougher surface of the PTB7-Th: DICTFDT film could lead to better contact with the top electrode, which is helpful for charge collection. Taking into consideration of the closer π-π stacking and better ordering of DICTFDT in solid state as well, the improved FF of the PTB7-Th: DICTFDT device can be reasonably explained.

4 Conclusions

5*H*-fluoreno[3,2-b:6,7-b']dithiophene based non-fullerene small molecular acceptors of DICTFDT and TFDTBR were prepared and characterized. In spite

of having similar energy levels to that of TFDTBR, DICTFDT presents closer π – π stacking capability and better ordering in solid state. When PTB7-Th was used as the polymer donor to fabricate polymer:non-fullerene acceptor BHJ PSCs, the DICTFDT based device gained a maximum PCE of 5.12%, a little bit higher than 3.95% for the TFDTBR based device. The main contribution of the higher performance is ascribed to the improved FF, which is consistent with the higher charge carrier mobility and more balanced charge transport within the PTB7-Th: DICTFDT device. With a proper choice of compatible polymer donor or further molecular engineering, DICTFDT could serve as an excellent non-fullerene acceptor for efficient PSCs.

Reference

[1] Chen J, Cao Y. Development of Novel Conjugated Donor Polymers for High-Efficiency Bulk-Heterojunction Photovoltaic Devices[J]. *Acc. Chem. Res*., 2009, 42(11): 1 709-1 718

[2] Cheng Y-J, Yang S-H, Hsu C-S. Synthesis of Conjugated Polymers for Organic Solar Cell Applications[J]. *Chem. Rev*., 2009, 109(11): 5 868-5 923

[3] Li G, Zhu R. Yang Y. Polymer Solar Cells[J]. *Nat. Photon*., 2012, 6(3): 153-161

[4] Dou L, You J, Hong Z *et al*. 25th Anniversary Article: A Decade of Organic/Polymeric Photovoltaic Research[J]. *Adv. Mate*r., 2013, 25(46): 6 642-6 671

[5] Li Y. Molecular Design of Photovoltaic Materials for Polymer Solar Cells: Toward Suitable Electronic Energy Levels and Broad Absorption[J]. *Acc. Chem. Res*., 2012, 45(5): 723-733

[6] Xiao S, Zhang Q, You W. Molecular Engineering of Conjugated Polymers for Solar Cells: An Updated Report[J]. *Adv. Mater*., 2017, 29(20): 1 601 391

[7] Liu T, Troisi A. What Makes Fullerene Acceptors Special as Electron Acceptors in Organic Solar Cells and How to Replace Them[J]. *Adv. Mater*., 2013, 25(7): 1 038-1 041

[8] He Y, Li Y. Fullerene Derivative Acceptors for High Performance Polymer Solar Cells[J]. *Phys. Chem. Chem. Phys*., 2011, 13(6):1 970-1 983

[9] Zhao J, Li Y, Yang G *et al*. Efficient Organic Solar Cells Processed from Hydrocarbon Solvents[J]. *Nat. Energ*y, 2016, 1: 15 027

[10] Lin Y, Li Y, Zhan X. Small Molecule Semiconductors for High-efficiency Organic Photovoltaics[J]. *Chem. Soc. Rev*., 2012, 41(11): 4 245-4 272

[11] Anthony J E. Small-Molecule, Nonfullerene Acceptors for Polymer Bulk Heterojunction Organic Photovoltaics[J]. *Chem. Mater.*, 2011, 23(3): 583-590

[12] Lin Y, Wang J, Zhang Z-G *et al*. An Electron Acceptor Challenging Fullerenes for Efficient Polymer Solar Cells[J]. *Adv. Mater*., 2015, 27(7): 1 170-1 174

[13] Lin Y, He Q, F Zhao *et al*. A Facile Planar Fused-Ring Electron Acceptor for As-Cast Polymer Solar Cells with 8.71% Efficiency[J]. *J. Am. Chem. Soc*., 2016, 138(9): 2 973-2 976

[14] Lin Y, Zhao F, Wu Y. Mapping Polymer Donors toward High-Efficiency Fullerene Free Organic Solar Cells[J]. *Adv. Mater*., 2017, 29(3): 1 604 155

[15] Cheng P, Zhang M, Lau T-K *et al*. Realizing Small Energy Loss of 0.55 eV, High Open-Circuit Voltage >1 V and High Efficiency >10% in Fullerene-Free Polymer Solar Cells via Energy Driver[J]. *Adv. Mater*., 2017, 29(11): 1 605 216

[16] Bin H, Zhang Z-G, Gao L *et al*. Non-Fullerene Polymer Solar Cells Based on Alkylthio and Fluorine Substituted 2D-Conjugated Polymers Reach 9.5% Efficiency[J]. *J. Am. Chem. Soc*., 2016, 138(13): 4 657-4 664

[17] Yang Y, Zhang Z-G, Bin H *et al*. Side-Chain Isomerization on an n-type Organic Semiconductor ITIC Acceptor Makes 11.77% High Efficiency Polymer Solar Cells[J]. *J. Am. Chem. Soc*., 2016, 138(45): 15 011-15 018

[18] Yao H, Chen Y, Qin Y *et al*. Design and Synthesis of a Low Bandgap Small Molecule Acceptor for Efficient Polymer Solar Cells[J]. *Adv. Mater*., 2016, 28(37): 8 283-8 287

[19] Baran D, Ashraf R S, Hanifi D A, *et al*. Reducing the Efficiency-stability-cost Gap of Organic Photovoltaics with highly Efficient and Stable Small Molecule Acceptor Ternary Solar Cells[J]. *Nat. Mater*., 2017, 16(3): 363-369

[20] Zhao W, Qian D, Zhang S, *et al*. Fullerene-Free Polymer Solar Cells with over 11% Efficiency and Excellent Thermal Stability[J]. *Adv. Mater*., 2016, 28(23): 4 734-4 739

[21] Li S, Ye L, Zhao W, *et al*. Energy-Level Modulation of Small-Molecule Electron Acceptors to Achieve over 12% Efficiency in Polymer Solar Cells[J]. *Adv. Mater*., 2016, 28(42): 9 423-9 429

[22] Liu T, Guo Y, Yi Y, *et al*. Ternary Organic Solar Cells Based on Two Compatible Nonfullerene Acceptors with Power Conversion Efficiency >10%[J]. *Adv. Mater*., 2016, 28(45): 10 008-10 015

[23] Zhao W, Li S, Yao H, *et al*. Molecular Optimization Enables over 13% Efficiency in Organic Solar Cells[J]. *Journal of the American Chemical Society*, 2017, 139(21): 7 148-7 151

[24] Holliday S, Ashraf R S, Nielsen C B, *et al*. A Rhodanine Flanked Nonfullerene Acceptor for Solution-Processed Organic Photovoltaics[J]. *J. Am. Chem. Soc*., 2015, 137(2): 898-904

[25] Gao J, Wang W, Zhang S, *et al*. Distinction between PTB7-Th Samples Prepared from $Pd(PPh_3)_4$ and $Pd_2(dba)_3$/P(o-tol)$_3$ Catalysed Stille Coupling Polymerization and the Resultant Photovoltaic Performance[J]. *J. Mater. Chem. A*, 2018, 6(1): 179-188

[26] Yang M, Lau T-K, Xiao S, *et al*. A Ladder-type Heteroheptacene 12H-Dithieno[2',3':4,5]thieno[3,2-b:2',3'-h]fluorene Based D-A Copolymer with Strong Intermolecular Interactions toward Efficient Polymer Solar Cells[J]. *ACS Appl. Mater. Interfaces*, 2017, 9(40): 35 159-35 168

[27] Lin Y, Zhang Z-G, Bai H, *et al*. High-performance Fullerene-free Polymer Solar Cells with 6.31% Efficiency[J]. *Energy Environ. Sci*., 2015, 8(2): 610-616